Electron density distribution in α-iron: A γ-ray diffraction study

W. Jauch
Hahn-Meitner-Institut, Glienicker Strasse 100, D-14109 Berlin, Germany

M. Reehuis
Max-Planck-Institut für Festkörperforschung, Heisenbergstrasse 1, D-70569 Stuttgart, Germany
(Received 24 July 2007; published 19 December 2007)

High-accuracy single-crystal structure factors, complete up to $\sin\theta/\lambda = 1.9$ Å^{-1} have been measured from α-iron at 295 K using 316.5 keV gamma radiation. A detailed description of the electron density distribution is presented in terms of a multipolar atomic deformation model. The charge asphericity due to preferential occupancy of the t_{2g} subshell is much smaller than that reported hitherto from x-ray measurements but is in quantitative agreement with *ab initio* calculations, laying to rest discussions about failures of theory in reproducing the aspherical charge. The $3d^7$ electron distribution in the solid is contracted by 8.9% relative to the free atom. The atomic radial scattering factor deduced from γ-ray diffraction is found to be in contradiction with earlier experimental and theoretical work. Achievement of a reliable Debye-Waller factor is of vital importance in this context. The directed metallic bonds are characterized by topological parameters at the bond critical points. Attention is paid to the 3*d*-4*s* occupation problem. A consistent interpretation of the 3*d* spin and charge form factors favors the occupation d^7 in the metal as against d^6 for the atom.

DOI: 10.1103/PhysRevB.76.235121 PACS number(s): 61.10.−i, 71.20.Be, 32.80.Cy

I. INTRODUCTION

The electron density distribution in a crystal, $\rho(\mathbf{r})$, is experimentally accessible from high-quality x-ray diffraction data. The diffracted intensities are connected with the structure factors, the discrete Fourier components of $\rho(\mathbf{r})$. The diffraction experiments are demanding since extremely accurate measurements are needed to move from standard crystal structure analysis toward addressing the rearrangement of the electron density due to binding in the solid. Though iron has been a subject of charge-density related experiments for a few decades now, the studies have been restricted either to reduced sets of low-order data or to the display of merely qualitative deformation-density features. In all cases, the major issue has been the comparison between experimental and theoretical scattering factors but a detailed examination of the resulting electron density is missing. There is thus the need for better and more extensive data. It is the purpose of this work to bridge this gap and to deduce an accurate charge density of crystalline iron from an extended set of structure factors by employing γ-ray Bragg diffraction.

Studies of crystals composed of heavier atoms demand a much higher accuracy than studies of compounds with lower atomic number, because the scattering from the valence electrons forms a smaller part relative to the dominating core contribution. Furthermore, the small unit cells encountered in highly symmetric elemental solids lead to only few reflections in the low order region where valence scattering is concentrated, calling again for an exceptional accuracy if meaningful information is to be obtained. These handicaps explain the rather limited number of available diffraction data in the case of the transition metals which in view of their importance clearly deserve more experimental attention.

The use of 316.5 keV gamma radiation offers two basic advantages to circumvent these obstacles for inorganic crystals with simple structures. The first advantage is the realization of the high-energy diffraction case (photon energy $\gg$ *K*-shell binding energy), thereby avoiding a number of experimental and theoretical sources of uncertainty in the process of deriving structure factors from the observed integrated intensities. The second advantage is brought about by favorable experimental conditions besides the high photon energy, such as the very narrow spectral spread of $\Delta\lambda/\lambda = 10^{-6}$, the perfect space-time stability of the wide homogeneous incident beam, or the absence of any optical device providing a simple instrumental resolution. It is noteworthy that the photon energy used in this work is considerably beyond 100 keV presently employed in synchrotron-radiation charge density studies.

The benefits offered by high-quality γ-ray structure factors data sets have been exploited and realized during the past years in exhaustive electron density studies on archetypal compounds such as the antiferromagnetic transition-metal monoxides and difluorides as well as on $SrTiO_3$.[1] The present work is a follow up to our recent investigation of chromium.[2] After the presentation of results, a detailed critical assessment of agreement and disagreement will be given with earlier results, deduced from laboratory x-ray, electron, and neutron diffraction work as well as from *ab initio* band-structure calculations.

II. EXPERIMENTAL AND DATA REDUCTION

The structural modification of pure iron at room temperature is called α-iron and has a body-centered-cubic (bcc) structure (space group $Im\bar{3}m$, $a = 2.866\,45(1)$ Å at 295 K),[3] in which each atom is surrounded by eight nearest neighbors along the cube diagonals and six next-nearest neighbors along the cube axial directions.

The single crystal used in the present investigation was a cube with dimensions of $2.480 \times 2.485 \times 2.565$ mm^3, pur-

chased from MaTecK/Jülich (Germany). Double-crystal γ-ray diffraction, using a perfect Si crystal as a collimator with an angular resolution of 1.5″, was employed to measure the diffraction profiles along three perpendicular directions. An isotropic angular full width at half maximum (FWHM) of around 30″ was found, and consequently, secondary extinction in the sample crystal is expected to be pronounced.

The diffraction data have been collected on the four-circle gamma-ray diffractometer installed at the Hahn-Meitner-Institut, where the most intense line of a ^{192}Ir source ($T_{1/2}$ =73.83 d) with a wavelength of 0.0392 Å (316.5 keV) is used. The flux at the sample position from a 200 Ci source amounts to 10^6 photons/s cm^2. The angular profiles of the diffraction peaks were recorded in ω-step scan mode (100 steps with length of 0.007°) with an intrinsic germanium detector. The data set, complete up to sin θ/λ=1.9 Å^{-1}, was collected at room temperature. The data collection lasted 10 weeks.

An absorption correction was carried out (μ =0.845 cm^{-1}),[4] resulting in a transmission range from 0.808 to 0.825. 380 diffraction data were measured corresponding to 89 independent reflections with an unprecedented counting-statistical overall precision of $\Sigma\sigma(I)/\Sigma I$=0.0030 for the averaged data. The absorption-weighted mean path lengths through the sample varied between 2.258 and 2.517 mm. It was therefore considered necessary to process each reflection with its individual path length in the calculation of the extinction correction and to treat symmetrically equivalent reflections separately. Data reduction was carried out using the XTAL suite of crystallographic programs.[5]

The data were corrected for the contribution of inelastic thermal diffuse scattering (TDS) from the acoustic phonons to the total intensity. The formalism of Skelton and Katz[6] was applied using the sound velocities from Ref. 7 and the instrumental parameters defining the sampled volume in reciprocal space: ω-scan peak width=0.5° and full circular detector window=0.46°. The maximum TDS contribution was 11%.

III. RESULTS

Structure refinements were performed with the program system VALRAY,[8] minimizing $\chi^2=\Sigma w(|F_o|^2-|F_c|^2)^2$, where F_o and F_c are the observed and calculated structure factors, respectively. The observations were weighted by their counting-statistical variances.

Except for Cr and Cu, the free 3d atoms have $3d^n4s^2$ electronic ground-state configurations. In going to the metal, the number of 4s electrons is no longer equal to 2, and the lowest state is commonly assumed to be close to $3d^{n+1}4s$ based on band theoretical results.[9] For metallic iron, important details include the following: (i) evaluation of the band structure for several configurations of the valence electrons indicated $3d^{7.0}4s^{1.0}$ to be the only stable one, for which self-consistency was obtained with the apparent Fermi level in the 3d and 4s bands at the same energy and[10] (ii) population analysis of the occupied d bands from the Green's function method gave a d-electron count of 6.78.[11] The energies of the two free atom configurations (d^6s^2 and d^7s^1) are so close together that an electron transfer from 4s to 3d is not surprising. Accordingly, the charge density analysis will be based on the atomic configuration $3d^74s$ ($^5F_5$) with the scattering factors calculated from the Hartree-Fock wave functions given in Clementi and Roetti.[12] However, implications of the occupation $3d^64s^2$ will also be paid attention for.

The diffraction data analysis is based on the classical form factor approximation of nonrelativistic scattering theory where corrections due to electron binding are neglected and where the Fourier transform relation between scattering amplitude and target distribution holds. A brief exposure of the relevance of relativistic effects is given in Ref. 2 and will not be repeated here.

A. Independent-atom model (IAM)

The fit parameters were the scale factor of the observed structure factors, a secondary extinction parameter using the Becker-Coppens formalism,[13] and the mean square vibrational amplitude. The observed structure factor contains a contribution from nuclear Thomson scattering, $f_N=(Ze)^2/Mc^2$. For iron, f_N=0.006 64 electron units, which has been accounted for. It turned out, however, that its inclusion has no substantial consequences ($\Delta\chi^2$=1.2 for the final multipole model). In order to reduce the influence of charge-density deformations in the outer shell, high-order refinements were carried out, taking into account only reflections with sin $\theta/\lambda>0.7$ Å^{-1}. The resulting scale factor was fixed in later refinements with improved scattering models.

B. Multipole model

In the aspherical atom multipole model, the electron density distribution is projected onto a small basis set of nucleus-centered real spherical harmonic functions with the local density rigidly following the motion of its associated nucleus.[14] The atomic density of Fe is represented by three components of the core, 3d spherical valence, and deformed valence electrons,

$$\rho_{\mathrm{Fe}}(\mathbf{r})=\rho_{\mathrm{core}}(r)+\kappa^3\rho_{3d}(\kappa r)+P_{\mathrm{hex}}\kappa^3\rho_{3d}(\kappa r)K_4(\mathbf{r}/r).$$

For site symmetry $m\bar{3}m$, the lowest nonvanishing higher pole is the Kubic harmonic $K_4(\mathbf{r}/r)$, which is a linear combination of y_{40} and y_{44+}.

The core density is the unperturbed Hartree-Fock (HF) electron density of the appropriate atomic orbitals. The square of the radial part of the 3d canonical HF orbitals is used to construct both the monopole and the hexadecapole. The κ parameter allows for expansion ($\kappa<1$) or contraction ($\kappa>1$) of the radial function. A single κ parameter is used for both the spherical valence shell and the deformation function. This constraint is necessary for the subsequent calculation of 3d-orbital occupancies (see Sec. IV B). P_{hex} is a variable population coefficient. The spherical surface harmonics are expressed relative to a global Cartesian frame which is oriented parallel to the unit cell axes.

In Table I, the quality of fit is given for the reference scattering models. The very high precision of the data is reflected by the large value of χ^2 for the IAM. A large im-

TABLE I. Quality of fit for the various $3d^7$ scattering models based on 380 observations; N_p=number of adjustable parameters. In all cases, the scale factor was fixed to the value obtained from a high-order refinement ($\sin\theta/\lambda > 0.7$ Å^{-1}).

	IAM	Monopole	Multipole
χ^2	4648	1536	1371
N_p	2	3	4

provement of fit is obtained with a spherical atom model allowing for a contraction of the $3d$ shell. Addition of the higher multipolar deformation leads to a further improvement of ~10% in χ^2. The data thus strongly support the multipole model, also reflected by the narrow confidence limits of the fit parameters which are listed in Table II. Yet, the actual value of χ^2 is considerably larger than the ideal one which should approach the number of degrees of freedom (for a complete model). Simple reasons for a large χ^2 are underestimated data uncertainties (lower limit set by counting statistics) or an error distribution with longer tails than a normal distribution. No systematic trend is revealed in the standardized residuals as a function of $\sin\theta/\lambda$. Finally, one should note that the statistical errors are related to the change in χ^2 when the parameters are varied away from the fitted values, and not to the absolute value of χ^2 itself.

The $4s$ form factor falls to immeasurably small values before the first Bragg reflection, so that the observations are insensitive to the $4s$ population which has been fixed to 1, and included in ρ_{core}.

Adjustment of the extinction parameter gave the best fit for a Lorentzian mosaic-spread distribution. The maximum reduction of $|F_o|^2$ is 38.8%, and a total of six independent reflections have a reduction of more than 5%. Tentative omission of the two most severely extinguished reflections affected only the mosaic and κ parameters which changed by less than two standard deviations, thus supporting the adequacy of the applied corrections. Extinction is further discussed in Sec. IV A.

The static model density, with the Debye-Waller factor omitted, was evaluated in direct space and proved to be positive everywhere which is the simplest condition the total electron density must satisfy. Figure 1 shows the static model deformation density (aspherical components only). The observed features exhibit magnitudes up to 0.8 e Å^{-3} about 0.24 Å from the nucleus. The charge asphericity will be further discussed in Sec. IV C.

Transition metal atoms require a multipole expansion at least up to $l=4$. Inclusion of one more symmetry-allowed term, y_{60} with a Slater-type radial dependence, led to no significant improvement in the least-squares fit, and so was discarded.

TABLE II. Mean square vibrational amplitude and multipole model parameters of α-Fe at room temperature. Reliability factors for the 380 observations: $R(F)=\Sigma|F_o-F_c|/\Sigma|F_o|=0.0050$ and $wR(F^2)=[\Sigma w(F_o^2-F_c^2)^2/\Sigma wF_o^4]^{1/2}=0.0102$.

U (Å^2)	0.00423(1)
κ	1.089(2)
P_{40} ($\lvert e\rvert$Å^4)	−0.220(23)

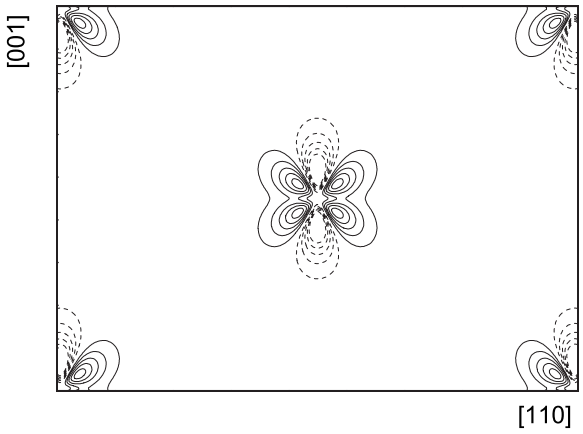

FIG. 1. Aspherical contributions to the static model density in the (110) plane. The density range is from −0.84 to 0.56 e Å^{-3}. Solid lines represent regions of excessive density and dashed lines depleted regions in steps of 0.1 e Å^{-3}. The zero contour is omitted. The densities are truncated at ±0.5 e Å^{-3}.

C. Metallic bond characteristics

The topological approach to chemical bonding[15] is a useful and convenient interpretation tool, according to which the interatomic interactions are characterized by local properties of the charge density at the bond critical saddle points $\mathbf{r}_c$ between two nuclei. There are basically two kinds of bonding interactions: shared-electron (covalent) interactions have $\nabla^2\rho(\mathbf{r}_c) \ll 0$, whereas closed-shell (ionic) interactions have $\nabla^2\rho(\mathbf{r}_c) \gg 0$. Metallic systems show a flat near-uniform electron density throughout the valence region, and the Laplacian is dominated by the positive curvature along the bond path, $\nabla^2\rho(\mathbf{r}_c) > 0$. A quantitative measure of the valence electron density flatness is provided by the ratio $r=\rho_{\min}(\mathbf{r})/\rho_{\max}(\mathbf{r}_c)$, where $\rho_{\min}(\mathbf{r})$ is the absolute minimum of the electron density and $\rho_{\max}(\mathbf{r}_c)$ the maximum density found at a bond critical point.[16] The flatness index r separates metals ($r \to 1$) from nonmetals ($r \to 0$).

Additional information about the bonding type is available from the local electron energy densities [$G(\mathbf{r}_c)$=kinetic energy density, $V(\mathbf{r}_c)$=potential energy density, and $H(\mathbf{r}_c) = G(\mathbf{r}_c) + V(\mathbf{r}_c)$=total energy density] that can be calculated from $\rho(\mathbf{r}_c)$ and $\nabla^2\rho(\mathbf{r}_c)$ using the approximation for $G(\mathbf{r}_c)$ proposed by Abramov[17] in combination with the local virial theorem from which $V(\mathbf{r}_c)$ can be estimated. For shared-electron interaction, there is a predominance of the (negative) local potential energy, so that $H(\mathbf{r}_c) < 0$, while for closed-shell systems $H(\mathbf{r}_c) \cong 0$ is observed.[1]

Table III summarizes the characteristics of the bond critical points of the static model electron density. There are closed-shell-type bonds [$\nabla^2\rho(\mathbf{r}_c) > 0$] between first and second neighbors with the distinguished features of a low electron density and a balance of the kinetic and potential energy densities. The flatness index has the value $r=0.634$, quite

TABLE III. Characteristics of the bond critical points. $\lambda_\parallel$ denotes the curvature of $\rho(\mathbf{r}_c)$ along the internuclear line (the two negative perpendicular curvatures are degenerate). Values of ρ in e Å^{-3} and values of $\nabla^2\rho(\mathbf{r}_c)$ and $\lambda_\parallel$ in e Å^{-5}. G, V, and G/ρ are given in a.u.

$\mathbf{r}_c$	$\rho(\mathbf{r}_c)$	$\nabla^2\rho(\mathbf{r}_c)$	$\lambda_\parallel$	$G(\mathbf{r}_c)$	$V(\mathbf{r}_c)$	$G(\mathbf{r}_c)/\rho(\mathbf{r}_c)$
$\frac{1}{4}, \frac{1}{4}, \frac{1}{4}$	0.227	2.57(1)	3.66	0.0279(2)	−0.0290(4)	0.829
$\frac{1}{2}, \frac{1}{2}, 0$	0.147	0.93(1)	1.07	0.0113(3)	−0.0129(6)	0.517

remote from the free-electron value of 1. The kinetic energy per electron, $G(\mathbf{r}_c)/\rho(\mathbf{r}_c)$, is found to be less than 1 (in a.u.), a property the metallic and the covalent bond have in common. Remarkably, the absolute values of the critical point parameters are essentially the same as those found in the case of chromium, also having bcc structure.[2]

IV. DISCUSSION

A. Extinction

The boundary between kinematical (intensity coupling) and dynamical (wave coupling) diffraction theories is set by the extinction length, $t_{\text{ext}}=V/(\lambda F)$ (V=unit cell volume, λ =wavelength, and F=structure factor in units of scattering length), and its magnitude with respect to the size of the perfect-crystal microdomains (called mosaic blocks). If they are not sufficiently small, then the incident beam is attenuated by coherent multiple scattering before it reaches the next mosaic block, that is, primary extinction occurs. The extinction coefficient y, defined as the ratio of the observed integrated intensity to its kinematical value, may be approximated ($y>0.5$) for primary type by the simple expression $y_p \approx \exp[-(\delta/2)^2]$, where δ is the average domain size in units of t_{ext}.[18] The coherent domains are expected to be of the order of 1 μm in diameter. In the present γ-ray study, the smallest value of t_{ext} is 57 μm for the 110 reflection. For a perfect block of thickness one-tenth of t_{ext}, the intensity is reduced by 0.25% relative to the kinematical value. Hence, if there were perfect regions of ~6 μm diameter, then primary extinction could introduce an apparent form factor error of ~0.1%. This has to be contrasted with $t_{\text{ext}}=3.2$ μm for Mo $K\alpha$ radiation, where primary extinction will necessarily occur, irrespective of the use of single-crystal or powder material (see Sec. IV D 1).

Secondary extinction, the other deviation from kinematical diffraction conditions, is due to incoherent multiple scattering from different mosaic blocks with the same orientation so that the incident beam does not remain constant but will be weakened as it traverses the crystal. Examination of the wavelength dependence of extinction by γ-ray diffraction in the energy range of 200–600 keV has confirmed and substantiated the validity of the standard theory of secondary extinction.[19,20]

The intensity reduction due to secondary extinction depends upon wavelength and specimen properties via the parameter $\lambda^2 T/\Gamma$ (T=absorption-weighted mean path length of diffracted beam and Γ=FWHM of mosaic distribution function for which generally a Lorentzian or Gaussian is assumed). It can be important even in γ-ray diffraction despite the very short wavelength, as relatively large samples are required to compensate the low crystal reflectivity. The high-resolution rocking curves, recorded with a perfect Si-crystal collimator, did not allow clear distinction between a Lorentzian and Gaussian shape, so that the choice was made on the basis of the chi-square statistic, and a preference for a Lorentzian mosaic distribution was found ($\Delta\chi^2=8.8\%$), yielding the refined width $\Gamma_L=12.4(1)''$ It is, however, the corresponding Gaussian width $\Gamma_G=32.8(2)''$, which reproduces the observed value of ~30″. The physical meaning of Γ_L thus appears to be dubious at first sight. The disparity in width, however, is not unexpected since the expressions described by Becker and Coppens[13] predict equal intensity losses for $\Gamma_L=0.48\Gamma_G$ under otherwise identical conditions. The relation $\Gamma_{\text{obs}}=\Gamma_G \approx 2\Gamma_L$ between observed and fitted mosaic spreads has been noted before in a study of MnF_2.[21]

B. Vibrational parameter

The mean-square amplitude of atomic vibrations obtained in this work, $U=0.004\,23(1)$ Å^2, is considerably smaller than the value reported by Ohba *et al.*[22] in their x-ray charge density study at 297 K, $U=0.005\,07(2)$ Å^2. It is known since a few years that the use of a graphite-monochromated Mo $K\alpha$ beam causes systematic intensity errors via scan-angle truncation.[23] Since the reflection width $\Delta\theta$ is linked to the wavelength dispersion $\Delta\lambda/\lambda$ by the relation $\Delta\theta=(\Delta\lambda/\lambda)\tan\theta$, the large wavelength window of the bremsstrahlung component is progressively truncated at higher Bragg angles, inevitably resulting in biased vibrational parameters that are systematically too large. Atomic displacement parameters were shown to increase by ~0.0006 and 0.0028 Å^2 for measurements with tube voltages of 50 and 25 kV, respectively, i.e., by an amount matching the observed discrepancy.[23] The spectral width of the 316.5 keV photon beam is $\Delta\lambda/\lambda=10^{-6}$ and no monochromator is needed.

Other experimental methods have also been used in the determination of the iron vibrational parameter at ambient temperature. From measurement of x-ray high-order powder reflections at two temperatures, $U=0.004\,32(13)$ Å^2 was obtained.[24] The values, 0.004 32, 0.004 22, and 0.004 18 Å^2, were calculated by Merisalo and Paakkari[25] from force constant models based on the results of inelastic neutron scattering measurements performed by three different experimental groups. There is thus remarkable agreement between the independent estimates of U.

The possible influence of anharmonic contributions to the Debye-Waller factor has been investigated. For $m\bar{3}m$ point

symmetry, there is one isotropic and one anisotropic quartic term in the Gram-Charlier expansion of the atomic probability density function. Combined multipole-anharmonicity refinement leads only to an insignificant improvement of fit. There is thus no noticeable anharmonic component in the atomic potential.

An adequate description of thermal motion is a necessary condition for a meaningful extraction of charge density information from the diffraction data. Validation of the thermal parameter is therefore an important issue lending support and credibility to the further conclusions.

C. Asphericity of charge distribution

The $3d$ electron density of a transition metal atom may be described by spherical harmonic functions or, alternatively, it may be expressed in terms of the orbital components of its atomic wave function. By equating the two descriptions of the density, a set of linear equations is obtained from which the orbital occupancies can be derived from the multipole populations ($l_{max}=4$).[26] With an octahedral environment, the atomic d orbitals split into doubly degenerate e_g and triply degenerate t_{2g} orbitals. In a bcc metal, the t_{2g} orbitals point toward the nearest neighbors along the body diagonal direction, while the e_g orbitals are directed toward the second nearest neighbors along the cube edges.

From the refined multipole parameters follows 62.5(3)% t_{2g} and 37.5(3)% e_g. Note that the same percentage is obtained by assuming six $3d$ electrons instead of seven. The population of the t_{2g} orbitals is thus larger than the 3:5 ratio, the value for a spherical charge distribution. The orbital occupancies are clearly reflected in the deformation map (Fig. 1) where the dominant features are electron buildup along $\langle 111 \rangle$, pointing toward the nearest neighbors, and electron depletion toward the second nearest neighbors. The experimental charge asphericity of α-Fe displayed by Ohba *et al.*[22] is qualitatively reproduced. The number of d electrons which contribute to the aspherical charge density is given as $Z_a = n(t_{2g}) - (\frac{3}{2})n(e_g)$, with n indicating the number of electrons having symmetry t_{2g} or e_g; the deduced value is $Z_a = 0.44(3)$.

In the bcc metals, there occur pairs of reflections with different wave vectors of equal magnitude such as (330/411) or (442/600), and differences of the intensity ratios from unity are a direct measure of the anisotropy in the charge density. From measurement of a couple of such reflections, the t_{2g} population in Fe was estimated to be 64.8(1.4)%;[22] in an earlier study[27] about 69% (no standard deviation is given) was found. There is thus agreement concerning a preponderance of t_{2g} over e_g charge density though the asphericity turns out to be smaller than that indicated by the earlier experiments, with the present work providing a substantial advance in accuracy.

A discrepancy between theory and experiment for the paired reflections has been considered a remaining problem in band structure calculations.[28] It is therefore important to compare the respective deviations from spherical symmetry. In Table IV, a number of form factor ratios are given, and it is seen that the ratios from the multipole model are fairly well reproduced by the calculations. Previous directly measured ratios are up to four times larger than the theoretical ones.[22] It is also noteworthy that Wakoh and Yamashita[11] predict a t_{2g} percentage which coincides with our observed value.

TABLE IV. Form factor ratios for paired reflections with scattering vectors of equal magnitude from the present multipole model and band structure calculations.

	Present study	Theor. (Ref. 34)	Theor. (Ref. 28)	Theor. (Ref. 33)
$f(330)/f(411)$	1.0033	1.0032	1.0031	1.0025
$f(431)/f(510)$	1.0052	1.0046		
$f(433)/f(530)$	1.0030	1.0025		
$f(442)/f(600)$	1.0072	1.0059	1.0060	
$f(532)/f(611)$	1.0048	1.0040		

Similarly, when discussing the charge asphericity in terms of Z_a, it was noted that the value derived from x-ray diffraction is twice that obtained from theory.[29] The disagreement has been connected to a basic failure of theory. In Ref. 29 (Fig. 3), the aspherical charge for Fe from theoretical data reads $Z_a=0.4$, which is the value found in the present work.

There is thus no disparity but rather substantial agreement between experiment and theory about the charge asphericity in α-iron.

D. Form factors

1. X-ray radial form factor

For the radial scaling parameter κ, a very pronounced deviation from the IAM is observed. The $3d^7$ valence shell exhibits a spatial contraction of 8.9%, which corresponds to a form factor expansion relative to the free atom. The atomic form factor f_{hkl} is related to the fitted structure factor F_{hkl} through $f_{hkl}=F_{hkl}/2$, so that for a monatomic crystal, the static values are simply obtained by multiplication with the inverse Debye-Waller factor. Absolute values of the atomic crystal scattering factor for the first 16 diffraction vectors are listed in Table V, where also the numerical contributions of both the core and valence electrons have been individually identified. Our experimentally derived values are now compared with earlier x-ray and electron diffraction measurements, performed on an absolute scale.

Paakkari and Suortti[30] used a powder sample and Mo $K\alpha$ radiation to measure the five lowest-order reflections, resulting in scattering factors (corrected for anomalous dispersion) that are reduced between 4.5% for $f(110)$ and 1.7% for $f(310)$ with respect to the values of the present study. The mean size of the powder particles was 3–5 μm. With perfect blocks of 2 μm diameter, primary extinction introduces systematic errors that perfectly match the observed discrepancies, though the coherent domain size has been claimed to be smaller by 2 orders of magnitude in Ref. 30.

Later, single-crystal experiments with Mo $K\alpha$ radiation were performed on a plate of 0.04 mm thickness.[31] The integrated intensities of the (110) and (200) reflections, ob-

TABLE V. Static scattering factors from the multipole model fit for α-iron in units of e/atom. f_{core} and $f_{valence}$ denote the contributions from the core and $3d^7$ valence electrons, respectively. f is the total contribution from all electrons. f_{IAM} is calculated from Ref. 12 for a $3d^74s^1$ independent atom, and f_{theory} is taken from Ref. 33.

hkl	$\sin\theta/\lambda$ (Å^{-1})	f_{core}	$f_{valence}$	f	f/f_{IAM}	f/f_{theor}
110	0.2467	15.130	3.886	19.016	1.018	1.039
200	0.3489	13.161	2.453	15.614	1.021	1.034
211	0.4273	11.728	1.677	13.405	1.024	1.025
220	0.4934	10.656	1.173	11.829	1.023	1.020
310	0.5516	9.840	0.810	10.650	1.020	1.017
222	0.6042	9.207	0.615	9.822	1.022	1.015
321	0.6527	8.707	0.432	9.139	1.018	1.013
400	0.6977	8.304	0.263	8.567	1.011	1.010
330	0.7400	7.974	0.215	8.189	1.014	1.010
411	0.7400	7.974	0.188	8.162	1.011	1.009
420	0.7801	7.698	0.129	7.827	1.011	1.008
332	0.8181	7.463	0.104	7.567	1.013	1.009
422	0.8545	7.260	0.051	7.311	1.010	1.007
431	0.8894	7.080	0.020	7.100	1.008	1.007
510	0.8894	7.080	–0.017	7.063	1.003	1.005
521	0.9554	6.773	–0.041	6.732	1.003	Not given

tained at different spots from the crystal surface, were plotted as a function of the reciprocal half-width. Extrapolation to infinite half-width gave crystal form factors, after correcting for anomalous dispersion, which are 9% smaller than our values. Besides extinction, surface irregularities are effective in decreasing the measured intensity.

High-energy electron diffraction allows determination of the structure factor for a first-order reflection by exploiting the critical-voltage effect. Owing to destructive interference, the intensity of the second-order reflection will show a minimum for a particular accelerating voltage. The first-order value is determined from the measured voltage by many-beam calculations covering higher-order Fourier coefficients for which the independent-atom approximation has to be assumed. Two x-ray scattering factors have been determined, $f(110)$ and $f(200)$, which are 3.6% and 2.7% smaller than the present values.[32] An important source of error of the critical-voltage method appears to be in the calculated second-order structure factors which in the present case are definitively affected by bonding (see Table V).

A comprehensive band-structure calculation for ferromagnetic iron was performed by Callaway and Wang,[33] who employed the self-consistent linear combination of Gaussian orbitals method, and used the computed wave functions to determine the x-ray form factor, tabulated up to $\sin\theta/\lambda = 0.9$ Å^{-1}. In Table V, it is shown that the three lowest-order values are 3.9%–2.5% smaller than the model fit values, while the deviation for the higher orders smoothly approaches 0.5%. The observed disagreement between theory and experiment therefore cannot be attributed to an inadequate experimental scaling factor. Rather, it is an indication that the d orbitals have a radial extension different from the predicted one. The charge density is more concentrated around the nuclei.

Other *ab initio* calculations, based on the augmented plane wave method[34] and the Green's function method,[28] gave quite similar results, with the low-order Fourier coefficients again smaller than the model fit values. The three theoretical studies are thus in substantial agreement with each other. Core and valence contributions to f have been given individually in Ref. 28, so that the source of discrepancy between theory and experiment can be identified unambiguously. There is agreement concerning the inner electrons, whereas the theoretical valence form factors appear to be systematically reduced in the order of 30%.

As in the case of Cr, the results from the literature share one common feature, that is, an apparent expansion of the valence charge distribution is found, whereas the γ-ray data require an opposite behavior, namely, a large contraction of the valence shell relative to the free atom.

2. The 3d-4s problem

Assuming the atomic ground state configuration $3d^64s^2$ ($^5D_4$) with Hartree-Fock wave functions from Clementi and Roetti[12] results in a deterioration of χ^2 by 6.4% relative to the metal electron configuration. The different d-electron counts are associated with different radial parameter values, $\kappa(d^6)=1.062(2)$ as compared to $\kappa(d^7)=1.089(2)$, to which correspond the following mean radii: $\langle r(d^6)\rangle=0.533$ Å and $\langle r(d^7)\rangle=0.578$ Å [$\langle r\rangle=\langle r\rangle_o/\kappa$, with the subscript denoting the IAM value]. Otherwise, it appears to be impossible to infer the number of $3d$ electrons in a direct way from the γ-ray diffraction data without extra information. The lowest-order Bragg reflection has $\sin\theta/\lambda=0.247$ Å^{-2}, so that the region where the scattering factor curves differ most is not accessible, with an inevitable loss of sensitivity.

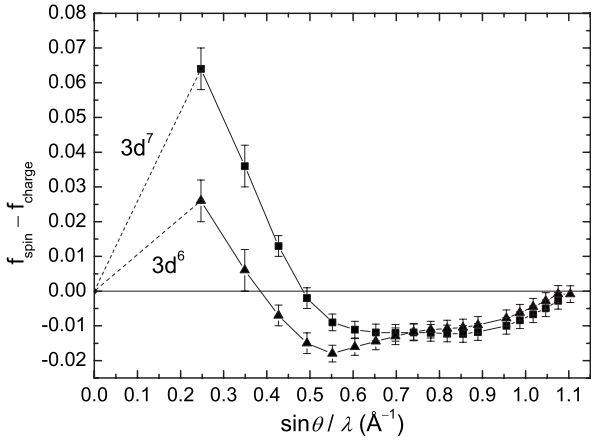

FIG. 2. The difference between the spherically averaged spin form factor ($=\langle j_o\rangle_{obs}$ from Ref. 38 and experimental uncertainties from Ref. 39) and the radial charge form factors for $3d^7(\kappa=1.089)$ and $3d^6(\kappa=1.062)$ as deduced from neutron and γ-ray diffraction. The form factors are normalized to unity at $\sin\theta/\lambda=0$.

The missing extra information is encoded in the average Coulomb potential (mean inner potential) of the total (nuclear and electronic) charge density in the unit cell. It is defined by $\Phi_0=(1/V)\int_{cell}\Phi(r)d^3r$, with the zero potential taken at infinity, outside the bounded crystal, and equals the zero Fourier component of the potential. The well-known Bethe formula reads $\Phi_0=(2\pi/3V)\Sigma_i^{cell}Z_i\langle r_i^2\rangle$, where $Z_i\langle r_i^2\rangle=\int r^2\rho_i(r)d^3r$ is the second moment of the electron density of an atom with atomic number Z_i.[35,36] Φ_0 is therefore primarily determined by the spatial distribution of the outer electrons and proportional to the diamagnetic susceptibility. For an IAM crystal, one finds $\Phi_0(3d^64s^2)=29.5$ V and $\Phi_0(3d^74s^1)=22.5$ V for the two configurations in question. Essentially, all the difference comes from the N shell, so that bonding effects in the real crystal play only a minor role. The large difference in Φ_0 suggests a possibility to resolve the $3d$-$4s$ problem directly by comparison with experimental values. For a number of materials, Φ_0 has been measured by electron interferometry. However, this technique seems to be impracticable for ferromagnets such as iron, and an experimental value of Φ_0 is missing in the literature.

3. Magnetic form factor

Complementary information about the spatial distribution of the unpaired $3d$ electrons is available from magnetic form factor measurements, possibly also throwing new light on the $3d$-$4s$ problem. The magnetic form factor of metallic iron has been extensively studied by Shull and Yamada[37] by means of elastic scattering of polarized neutrons. The asphericity of the spin density is found to be inverse to that of the charge density, with the unpaired spin population showing an e_g occupation of 53(1)%. A quantitative comparison between charge and spin form factor must therefore rely on the spherically averaged components. In Fig. 2, the comparison is shown for a single $3d$ electron from the two different atomic configurations under consideration. As it can be seen, there are substantial systematic differences between f_{spin} and f_{charge}. One should realize, however, that the two form factors have somehow different origins, to be discussed further below, and their simultaneous interpretation is not as straightforward as one might suppose.

In the ordinary Hartree-Fock method, electrons in the same shell but differing in spin are required to have the same radial wave function. This constraint is relaxed in the unrestricted HF (UHF) method for open-shell systems, which allows different radial functions for electrons with opposite spin, i.e., $R_{nl\alpha}\neq R_{nl\beta}$. For an atom with unbalanced spin, electrons with α or β spin will experience unequal α-α and β-β exchange interactions $[N_{3d}(\alpha)-N_{3d}(\beta)=2.2$ for ferromagnetic iron]. Since the exchange interaction is attractive, the majority (α) spin functions will show a contraction relative to the β-spin counterparts. For atomic Fe ($^5D_4$), the $\langle r\rangle$ values found from an accurate UHF wave function are $\langle r_{3d}(\alpha)\rangle=0.560$ Å and $\langle r_{3d}(\beta)\rangle=0.614$ Å, whereas the restricted HF value, $\langle r_{3d}\rangle=0.568$ Å, is the weighted mean of the former two values.[40]

According to the κ parametrization (length scaling), a contraction of the α-spin density relative to that of the total charge implies $f_{spin}(\kappa+\Delta\kappa)\geqslant f_{charge}(\kappa)$. Seemingly, this property is reflected in Fig. 2 by the large positive differences in the low-order region where better "agreement" is achieved for the d^6 configuration. Because of the sign reversal at medium $\sin\theta/\lambda$, however, spin and charge density cannot be made to agree closely by a single scaling parameter $\Delta\kappa$.

It is remarkable that the integrated difference between the scattering factor curves vanishes for the $3d^6$ configuration, whereas a positive value remains for $3d^7$. A clue to the origin of this finding is offered by the Silverman-Obata sum rule[41] which connects the spherical form factor with the average value of r^{-1}: $\int_0^\infty f(q)dq=(\pi/2)\langle r^{-1}\rangle$. As an obvious consequence, both the spin and charge distribution would have the same mean extension in the d^6 configuration, contrary to the expectation outlined above. On the other hand, the predicted inequality $\langle r^{-1}\rangle_{spin}>\langle r^{-1}\rangle_{charge}$ is satisfied for d^7, so that this occupation number must be regarded as the more proper one. From closer inspection of Fig. 2, $\langle r^{-1}\rangle_{spin}-\langle r^{-1}\rangle_{charge}\cong 0.007$ Å^{-1}, which should be compared with $\langle r^{-1}\rangle_{charge}=\kappa\langle r^{-1}\rangle_o=2.387$ Å^{-1}, calculated from the HF d^7 wave function.[12]

One should note at this point that form factor differences are intimately related to energy differences. Since the electron-nucleus electrostatic energy, $-Ze^2\langle r^{-1}\rangle$, is by far the dominant contribution to the potential energy of the electronic charge distribution, the virial theorem for Coulombic systems indicates that it is approximately equal to twice the total electronic energy. A compensation of positive and negative differences, as observed for d^6, thus corresponds to a vanishing change in total energy ΔE $(=E_{spin}-E_{charge})$. In the same way follows from the positive integrated difference for d^7 a lowering in energy of the α electrons, $E_{spin}<E_{charge}$, as a consequence of the exchange interaction.

Joint interpretation of the charge and spin form factor has thus revealed distinctive features associated with the two integer occupation numbers of the $3d$ electrons. Only the occupation $3d^7$ is consistent with the general behavior predicted by the UHF method.

V. CONCLUDING REMARKS

An extended set of high-quality structure factors, achieved by the use of 316.5 keV gamma radiation, has provided the currently best possible representation of the electron distribution in α-Fe. Important findings include the following: (i) validation of data quality and scale factor estimate by comparison with available values of the thermal vibrational parameter; (ii) as in the case of chromium, the 3*d*-shell exhibits a pronounced contraction relative to the free atom; (iii) the charge asphericity is small with a slight preference for t_{2g} toward the nearest neighbors; (iv) directional metallic bonding features are quantitatively characterized in terms of electron density properties; (v) consistency between the expected behavior of charge and spin form factor is achieved with the occupation d^7 rather than d^6; and (vi) no indication for a failure of the localized 3*d* electron model is noticed. Finally, it should be emphasized that the high accuracy of the present method serves as a sensitive and useful test of *ab initio* calculations. The charge asphericity shows pleasing agreement between theory and experiment, but the revealed deviations in the radial extent of the valence density underline the need for improved theoretical treatments.

ACKNOWLEDGMENTS

We thank H.-J. Bleif for helpful discussions. Support from the Deutsche Forschungsgemeinschaft (Grant No. UL164/4) is acknowledged.

[1] W. Jauch and M. Reehuis, Phys. Rev. B **65**, 125111 (2002); **67**, 184420 (2003); **70**, 195121 (2004); W. Jauch, Acta Crystallogr., Sect. A: Found. Crystallogr. **A60**, 264 (2004); W. Jauch and M. Reehuis, *ibid.* **A61**, 411 (2005).
[2] W. Jauch and M. Reehuis, Phys. Rev. B **73**, 085102 (2006).
[3] T. C. W. Mak and G.-D. Zhou, *Crystallography in Modern Chemistry: A Resource Book of Crystal Structures* (Wiley, New York, 1997).
[4] J. H. Hubbell and S. M. Seltzer, National Institute of Standards and Technology Internal Report No. 5632, 1995 (http://www.physics.nist.gov/PhysRefData/XrayMassCoef/cover.html).
[5] *Computer Code XTAL 3.4; User's Manual*, edited by S. R. Hall, G. S. D. King, and J. M. Stewart (University of Western Ausralia, Perth, Australia, 1995).
[6] E. F. Skelton and J. L. Katz, Acta Crystallogr., Sect. A: Cryst. Phys., Diffr., Theor. Gen. Crystallogr. **A25**, 319 (1969).
[7] G. W. C. Kaye and T. H. Laby, *Tables of Physical and Chemical Constants*, 15th ed. (Longman, London, UK, 1993).
[8] R. F. Stewart, M. Spackman, and C. Flensburg, *Computer Code VALRAY; User's Manual* (Carnegie-Mellon University, Pittsburgh, Pennsylvania/University of Copenhagen, Copenhagen, Denmark, 2000).
[9] R. E. Watson, M. L. Perlman, and J. F. Herbst, Phys. Rev. B **13**, 2358 (1976).
[10] F. Stern, Phys. Rev. **116**, 1399 (1959).
[11] S. Wakoh and J. Yamashita, J. Phys. Soc. Jpn. **25**, 1272 (1968).
[12] E. Clementi and C. Roetti, At. Data Nucl. Data Tables **14**, 177 (1974).
[13] P. J. Becker and P. Coppens, Acta Crystallogr., Sect. A: Cryst. Phys., Diffr., Theor. Gen. Crystallogr. **A31**, 417 (1975).
[14] R. F. Stewart, Acta Crystallogr., Sect. A: Cryst. Phys., Diffr., Theor. Gen. Crystallogr. **A32**, 565 (1976).
[15] R. F. W. Bader, *Atoms in Molecules: A Quantum Theory* (Clarendon, Oxford, 1990).
[16] P. Mori-Sánchez, A. Martín Pendás, and V. Luaña, J. Am. Chem. Soc. **124**, 14721 (2002).
[17] Yu. A. Abramov, Acta Crystallogr., Sect. A: Found. Crystallogr. **A53**, 264 (1997).
[18] P. Suortti, Acta Crystallogr., Sect. A: Cryst. Phys., Diffr., Theor. Gen. Crystallogr. **A38**, 642 (1982).
[19] A. Palmer and W. Jauch, Acta Crystallogr., Sect. A: Found. Crystallogr. **A51**, 662 (1995).
[20] W. Jauch and A. Palmer, Acta Crystallogr., Sect. A: Found. Crystallogr. **A58**, 448 (2002).
[21] W. Jauch, A. J. Schultz, and J. R. Schneider, J. Appl. Crystallogr. **21**, 975 (1988).
[22] S. Ohba, Y. Saito, and Y. Noda, Acta Crystallogr., Sect. A: Cryst. Phys., Diffr., Theor. Gen. Crystallogr. **A38**, 725 (1982).
[23] B. Rousseau, S. T. Maes, and A. T. H. Lenstra, Acta Crystallogr., Sect. A: Found. Crystallogr. **A56**, 300 (2000).
[24] T. Paakkari, Acta Crystallogr., Sect. A: Cryst. Phys., Diffr., Theor. Gen. Crystallogr. **A30**, 83 (1974).
[25] M. Merisalo and T. Paakkari, MRS Bull. **8**, 195 (1973).
[26] A. Holladay, P. Leung, and P. Coppens, Acta Crystallogr., Sect. A: Cryst. Phys., Diffr., Theor. Gen. Crystallogr. **A38**, 563 (1982).
[27] M. Diana and G. Mazzone, Phys. Rev. B **18**, 6631 (1978).
[28] S. Wakoh and J. Yamashita, J. Phys. Soc. Jpn. **30**, 422 (1971).
[29] C. Petrillo, F. Sacchetti, and G. Mazzone, Acta Crystallogr., Sect. A: Found. Crystallogr. **A54**, 468 (1998).
[30] T. Paakkari and P. Suortti, Acta Crystallogr. **22**, 755 (1967).
[31] M. Diana and G. Mazzone, Phys. Rev. B **9**, 3898 (1974).
[32] O. Terasaki, Y. Uchida, and D. Watanabe, J. Phys. Soc. Jpn. **39**, 1277 (1975).
[33] J. Callaway and C. S. Wang, Phys. Rev. B **16**, 2095 (1977).
[34] P. D. De Cicco and A. Kitz, Phys. Rev. **162**, 486 (1967).
[35] J. L. Birman, Phys. Rev. **98**, 1863 (1955).
[36] M. O'Keeffe and J. C. H. Spence, Acta Crystallogr., Sect. A: Found. Crystallogr. **A50**, 33 (1994).
[37] C. G. Shull and Y. Yamada, J. Phys. Soc. Jpn. **17**, 1 (1962).
[38] S. Kaprzyk, B. van Laar, and F. Maniawski, J. Magn. Magn. Mater. **23**, 105 (1981).
[39] C. G. Shull, quoted by P. D. De Cicco and A. Kitz, in Ref. 34.
[40] P. S. Bagus and B. Liu, Phys. Rev. **148**, 79 (1966).
[41] J. N. Silverman and Y. Obata, J. Chem. Phys. **38**, 1254 (1963).